

# Efficient Model-Based Quantification of Left Ventricular Function in 3-D Echocardiography

Olivier Gérard\*, Antoine Collet Billon, Jean-Michel Rouet, Marie Jacob, Maxim Fradkin, and Cyril Allouche

**Abstract**—Quantitative functional analysis of the left ventricle plays a very important role in the diagnosis of heart diseases. While in standard two-dimensional echocardiography this quantification is limited to rather crude volume estimation, three-dimensional (3-D) echocardiography not only significantly improves its accuracy but also makes it possible to derive valuable additional information, like various wall-motion measurements. In this paper, we present a new efficient method for the functional evaluation of the left ventricle from 3-D echographic sequences. It comprises a segmentation step that is based on the integration of 3-D deformable surfaces and a four-dimensional statistical heart motion model. The segmentation results in an accurate 3-D + time left ventricle discrete representation. Functional descriptors like local wall-motion indexes are automatically derived from this representation. The method has been successfully tested both on electrocardiography-gated and real-time 3-D data. It has proven to be fast, accurate, and robust.

**Index Terms**—Deformable surfaces, four-dimensional statistical modeling, left ventricle function quantification, three-dimensional echocardiography.

## I. INTRODUCTION

**E**CHOCARDIOGRAPHY has become a major modality in the diagnosis of heart diseases due to its innocuousness, the relatively low cost and small size of equipment compared to other modalities, and its ability to reveal the anatomy and to give functional information in real-time. Current exams are based on the interpretation of a two-dimensional (2-D) image time series, obtained from standard orientations (between the ribs or through the esophagus). Today's commercially available three-dimensional (3-D) equipment performs the acquisition of a series of 2-D image sequences at different angular positions, via small motor-driven rotations of the image plane over 180°. After image acquisition, a series of 3-D sets over one cardiac cycle is reconstructed, using the images' echocardiogram (ECG) tags and their angular positions. The whole procedure typically requires several minutes, which makes it subject to artifacts caused by heart motion and irregular heartbeat. Real-time 3-D, which overcomes these limitations, requires the development of 2-D piezomatrices with embedded electronics capable of parallel beamforming, which is a difficult technological challenge. Yet one can expect that this technology will

become ubiquitous soon. For instance, Philips Medical System Ultrasound—Andover has recently launched on the market a real-time 3-D system that does not compromise image quality.

There is no doubt that 3-D increases the benefits of echocardiography, in particular in the quantification of the heart function [1]. A frequent indication for ultrasound examination in cardiology is the assessment of the left ventricle (LV), which is affected by coronary artery diseases and a number of cardiomyopathies. In standard 2-D echocardiography, this quantification is limited to a rather crude volume estimation derived from one or two images and a coarse model of the LV shape; clearly more accurate volume measurements can be expected from 3-D data [2]. Even more interesting are the new possibilities that 3-D opens in the estimation of the location and extent of ischemic damages, which can be derived from the quantification of the kinetics of the LV [3]. Another benefit is the better reproducibility of 3-D-based quantification, an area where 2-D echo is at deficit compared to the other modalities.

A prerequisite to the quantification of the LV is the identification of the inner border of the LV (also known as the endocardium). Considering the large amount of data per exam produced by real-time 3-D, manual outlining or other user-guided 2-D based techniques are not compatible with the clinical routine and have to be discarded. Indeed, a fast and robust segmentation tool with a high degree of automation is required. This is a challenge because despite the improvements of image quality in the last few years, like tissue harmonic imaging, ultrasound data still exhibit some serious adverse characteristics. In particular, there are large variations of image quality between patients; for instance, the external wall of the LV is frequently hardly visible in the images. Also, the spatial resolution is not isotropic and varies with the position in the data. Among other artifacts, there is a strong speckle noise superimposed on tissues echoes.

However, there is evidence that incorporating a priori information about cardiac anatomy, cardiac physiology, and data acquisition in the segmentation procedure can help a great deal in reaching a satisfactory level of robustness and speed of execution [3]–[5]. The 3-D size and shape characteristics of the LV, and its deformation over a cardiac cycle, are relatively consistent and can be fairly well characterized by specific models. Also, the accuracy that is required to properly assess its function is known, as are the possibilities of the imaging modality. Lastly, the geometry of data acquisition relative to the heart provides information about the local data characteristics. In this paper, we present an approach that takes advantage of this a priori knowledge.

Fig. 1 shows a flowchart of the successive operations of our quantification tool.

Manuscript received November 5, 2001; revised July 6, 2002. Asterisk indicates corresponding author.

\*O. Gérard is with the Medisys Group, Philips Research France, 51 rue Carnot, 92156 Suresnes, France (e-mail: Olivier.Gerard@philips.com).

A. Collet Billon, J.-M. Rouet, M. Jacob, and M. Fradkin are with the Medisys Group, Philips Research France, 92156 Suresnes, France.

C. Allouche was with the Medisys Group, Philips Research France, 92156 Suresnes, France.

Digital Object Identifier 10.1109/TMI.2002.804435

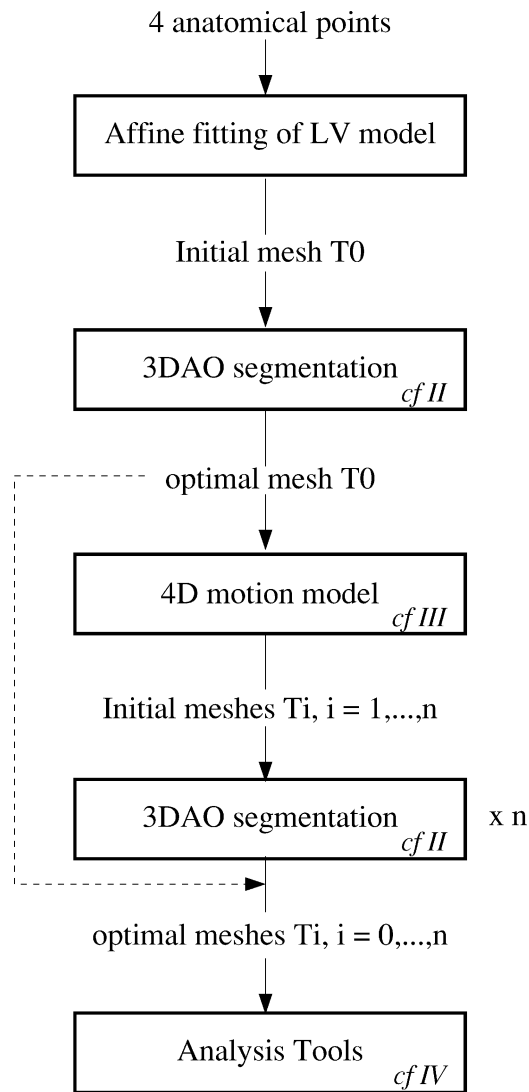


Fig. 1. Flowchart of the proposed method.

The user starts by identifying a handset of anatomical landmarks (three on the mitral valve and one at the apex) in the first 3-D set. These points determine an affine transform that properly aligns and scales a predetermined normal LV mesh, hence giving a fairly accurate approximation of the LV shape. Then, it is deformed using the 3-D active object (3DAO) segmentation technique, as explained in Section II.

To initialize the operation for the other 3-D datasets (i.e., for the other time frames) of the cardiac sequence, the classical solution consists in iteratively propagating the result obtained in the previous set [6]. As the motion of the LV between the successive 3-D sets can be fairly large, this initialization is inaccurate.

In our approach, we calculate an initial mesh for each 3-D set of the sequence using a motion model of the normal movement of the LV over a cardiac cycle, which operates on the result of the first segmentation. The motion model has been obtained from tagged MR studies and is described in Section III. It leads to an accurate initialization, usually very close to the endocardium. This level of accuracy is important because the deformation is all the more fast as the required subsequent deformation is small.

Then, these initial meshes are deformed independently using the 3DAO segmentation technique, and eventually they match the LV endocardium in the data series. This independent deformation strategy is particularly interesting when dealing with pathological LV motion.

One advantage of this model-based initialization is that the cardiac deformation model provides a one-to-one correspondence between the vertices of the meshes that is derived from biomechanical knowledge. This allows a better estimation of the wall motion than the sole mesh radial deformation, as is described in [7]. The analysis part that covers computation and display of wall-motion information is presented in Section IV. The successive steps of the proposed method (see also Fig. 1) are illustrated with transesophagus 3-D echocardiographic data.

Section V shows results obtained with ECG-gated and real-time 3-D acquisitions.

## II. ACTIVE-OBJECT-BASED SEGMENTATION

To analyze the four-dimensional (4-D) heart motion from ultrasonic images, one needs a fast and accurate segmentation tool. A number of methods for 3-D heart modeling have been reported in the literature. An excellent review of this topic can be found in [4]. Among these methods, deformable models have been successfully applied for medical image segmentation [8], [9]. Deformable models use either continuous, generally parametrized, surface representations such as superquadrics [10] or B-snakes [11] or discrete representations like triangulations [12], two-simplex meshes [13], or spring-mass models [14]. The robustness of deformable models can be improved by the integration of a priori knowledge of the organ of interest using a statistical shape model [15], [16] or appearance model [17], as well as image-acquisition specific characteristics.

We have used 3-D deformable models known as two-simplex meshes. Such models are suited to heart modeling because the heart shape is rather simple, and a small number of vertices (typically 500) carries enough information on the myocardium's shape and position. In the following, we first describe the mesh geometry, then explain how the mesh is deformed in order to fit the data. Finally, we discuss the deformation strategy used to segment the LV in ultrasonic images.

### A. Two-Simplex Geometry

A two-simplex mesh (SM) is a discrete closed surface model where each vertex is linked to three and only three neighbors (see Fig. 2). The SM-topology is the dual of a triangulation.

SM-geometry is fully described by four parameters at each vertex: the simplex angle  $\Phi$ , which characterizes the elevation of a vertex with respect to the plane defined by its three neighbors; and the barycentric coordinates  $\{\epsilon_1, \epsilon_2, \epsilon_3\}$  of the projection of a vertex onto its neighbor's plane. The direction normal to the latter plane defines the local surface's normal  $\mathbf{n}$ . An internal energy that is usually related to the mesh smoothness is derived from the spatial configuration of points. Hence, from these four parameters, it is possible to assign a contribution of each vertex to the internal energy of the mesh. More precisely, for each vertex position  $p$ , a position  $\hat{p}_i$  where the internal energy is minimal can be found. The difference between  $p$  and  $\hat{p}_i$

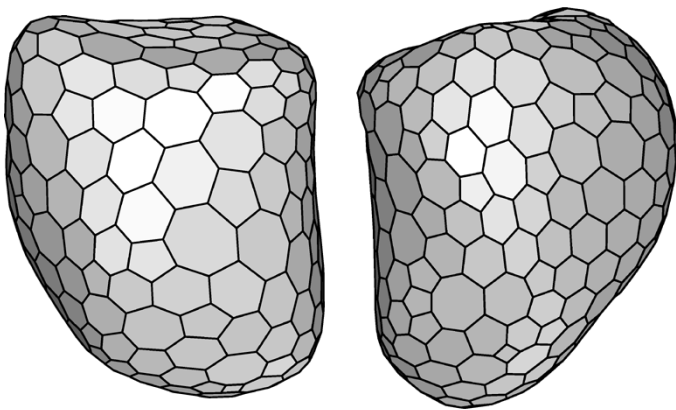


Fig. 2. Example of a two-simplex mesh (front and back view). This mesh approximates an LV and can be used as an initialization for the first segmentation process.

positions is then considered as an internal force  $F_{\text{int}}$ , which is later used in the iterative evolution (5)

$$F_{\text{int}} = \hat{p}_i - p. \quad (1)$$

Different kinds of internal energies have been studied and discussed in [13]. For LV segmentation, as the heart shape can be considered as smooth, we have chosen internal forces that minimize the local mesh curvature.

The deformation process (segmentation) is preceded by a mesh initialization step. For the segmentation of the LV, we usually start from an SM heart model, if available, or simply from a sphere or an ellipsoid. This first mesh is manually oriented and positioned into the dataset.

Some basic operations allow one to modify, either locally or globally, the mesh resolution (i.e., the mean area of the facets). This includes face splitting (refinement) and merging (decimation). One original advantage of our implementation is that the face resolution can be either manually controlled or automatically adapted during the mesh deformation process. This method is based on statistical analysis of the mesh resolution and on its local adaptation to image features.

### B. External Forces Computation

For each vertex  $p$ , we want to find the location that best fits the image. In practice, vertices are naturally dragged toward regions where the gradient of the image is high. As a search in 3-D is time consuming, we restrict the search along the direction of the vertex normal  $\mathbf{n}$ . Moreover, restricting the influence of the external forces to the normal direction leads to more reliable mesh deformations with respect to shape conservation and does not restrict the class of surface deformation [18]. A range  $r$  on the normal line controls the extent of the search space for the external forces calculation (see Fig. 3). For LV segmentation in ultrasound (US) images, a typical search range value is  $r = 15$  mm, but it can be manually set as well, depending on the quality of the initialization.

We found that for US images, a simple approximation of the gradient along a line such as the difference step by step of the voxel intensities greatly speeds up the process without any no-

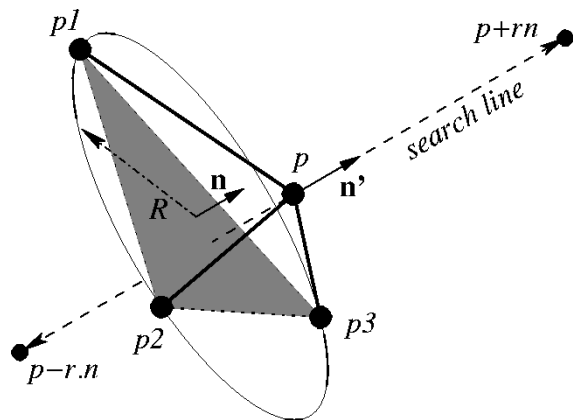


Fig. 3. Search line and range definition for external forces on a vertex.

tionable loss of segmentation accuracy. Hence the optimal position  $\hat{p}_e$  for a vertex  $p$  on the search line is the one that satisfies

$$\hat{p}_e = p + k.\mathbf{n}', \text{ where } k = \arg \max_{k \in [-l, l-1]} G(p, k) \quad (2)$$

given that the search range interval on the search line is decomposed using a Bresenham-like algorithm (like the one used in [19]) with an index  $k$  varying in  $[-l, l-1]$ , and a step vector  $\mathbf{n}'$  collinear to the normal  $\mathbf{n}$ .  $G(p, k)$  represents then the intensity difference in image  $I$ , and

$$G(p, k) = I(p + (k + 1).\mathbf{n}') - I(p + k.\mathbf{n}'). \quad (3)$$

With this formulation, we look for a point with the largest increase of intensity (which corresponds to a black object with a bright boundary, like a heart chamber in echography). For each vertex, we assign a confidence coefficient  $w_p$  ranged in  $[0, 1]$ . Depending on the increase of intensity found, this coefficient is assigned from an S-curve; one corresponds to large intensity increases, while  $w_p$  is close to zero when  $\hat{p}_e$  corresponds to a location where the intensity difference is too small, i.e., on the order of the local noise. Moreover, as the inner part of the heart is dark in the US images, we also eliminate points where the gray value  $I(p + k.\mathbf{n}')$  is too bright, thus preventing the mesh from going toward the very bright regions of the image. In this case, the confidence coefficient  $w_p$  is set to zero. Even if our formulation may be sensitive to noise and particularly speckle, it is very fast since no global 3-D gradient computation is required, and noise adverse effects are limited by internal force regularization.

Finally, after the optimal positions have been found, the external force  $F_{\text{ext}}$  can be expressed as

$$F_{\text{ext}} = w_p(\hat{p}_e - p). \quad (4)$$

### C. Deformation Strategy

A typical approach for mesh deformation, and therefore image segmentation, consists in applying a Newtonian mechanical model using (1) and (4) with a damping factor  $\gamma$

$$m \frac{\partial^2 p_i}{\partial t^2} = -\gamma \frac{\partial p_i}{\partial t} + F_{\text{int}} + F_{\text{ext}}. \quad (5)$$

In practice, the mass  $m$  of the vertices is equal to one, as well as the time step. This simplification is not restrictive as long as we allow some scaling of external and internal forces [13]. Thus a discrete implementation of (5) results in a Lagrangian model

$$p^{t+1} = p^t + (1 - \gamma)(p^t - p^{t-1}) + \alpha F_{\text{int}} + \beta F_{\text{ext}}. \quad (6)$$

In a pure local deformation, this Lagrangian evolution equation can be applied synchronously to all vertices, where  $p^t$  is the position of a vertex at time  $t$ , and  $\alpha$  and  $\beta$  are the weighting factors that control the balance between mesh regularity and data fitting.

To improve the segmentation robustness and convergence speed, a coarse-to-fine strategy is implemented in three steps:

- 1) manual placement of a coarse mesh;
- 2) mesh deformation with a few degrees of freedom that restricts it to rigid body, similarity, or affine transforms;
- 3) local deformations.

In step 1), we start with a coarse heart model that is properly positioned by aligning the mitral valve plane and the apex defined with four anatomical landmarks). Step 2) consists in constraining the apparent motion of each vertex with a global transform  $T$  (rigid-body; similarity—translation, rotation, and isotropic scaling; or affine transform). The parameters of this transform are derived from the minimization of the mean square error:  $\sum_p w_p \|T(p) - \hat{p}_e\|^2$ . For the LV segmentation, we usually use similarity and affine transforms. This step is very fast, and if the approximation looks good enough, the user can reduce the search range  $r$  and therefore speed up the whole process.

Finally, step 3), which is a free deformation, corresponds to the evolution (6). This step can also be considered as a coarse-to-fine algorithm since it gradually increases the mesh resolution as the deformation is iterated.

As an illustration, Fig. 4 gives an example of the overall deformation process, starting simply from a sphere (instead of a LV shape), showing the intermediary affine transform [step 2)] and the final results on two orthogonal views.

Real-time interactive tools have also been devised to let the user correct the result. These tools comprise 3-D mesh dragging toward a point on a hand-drawn curve, and mesh cutting.

Finally, using adequate external force computations, we have successfully tested this segmentation technique with other modalities like magnetic resonance imaging (MRI), computed tomography scans, and 3-D-rotational angiography.

#### D. From 3-D to 4-D

As explained above, we use an average LV model to initialize the mesh prior to the deformation. This initialization is based on four anatomical landmarks, which are identified in the data by the user. Repeating this operation in the whole series of 3-D sets would be time consuming and tedious. Alternately, provided that one of the data sets has already been segmented, one could initialize the 3DAO in the next data set with the result of the segmentation in the previous one. However, the deformation of the LV between two successive data sets can be quite large; therefore the simple duplication of the previous result can lie far from the endocardium. In our approach, we use a 4-D cardiac

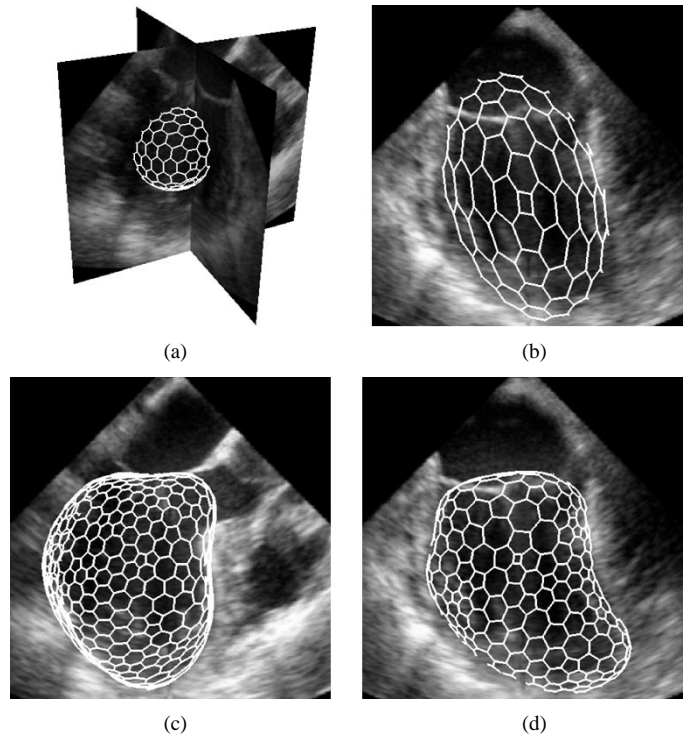


Fig. 4. Example of the deformation/segmentation process, (a) starting from a spherical mesh and (b) using an affine fitting. (c) and (d) show two orthogonal views of the segmentation result.

model that describes the motion of a beating LV over the cardiac cycle. The model and the data are synchronized with the ECG information, and at a given sampling time the modeled motion is applied to the result of the segmentation of one data set, leading to the desired initialization. The motion model is described in Section III and illustrated by results obtained with 3-D echocardiographic data.

### III. MR TAGGING-BASED DEFORMATION MODEL

In this section, we describe how we model the kinetics of the LV endocardium by a geometric deformation with a small number of parameters, independent of the variability of the LV shape. This model has been obtained from tagged MRI datasets, as described below.

#### A. MRI Tagging Data

Magnetic resonance tagging has proven its high ability to acquire the cardiac motion. Fisher *et al.* [20] introduced, in 1993, a new protocol, known as complementary spatial modulation of magnetization (CSPAMM), which makes it possible to acquire a complete cardiac cycle with a high and constant contrast. Stuber *et al.* [21] improved it by adding an efficient slice following technique.

We used this resulting protocol, CSPAMM-SF, on a Philips Gyroscan 1.5 T. Acquisitions were performed on 12 healthy volunteers (nine males and three females, aged 25–35), scanned in the same conditions by one operator. The basal slices were positioned 10 mm below the valves and the apical slices 10 mm above the radiological apex [22]. The longitudinal slice corresponded to the 2-D four-chamber echocardiographic view.

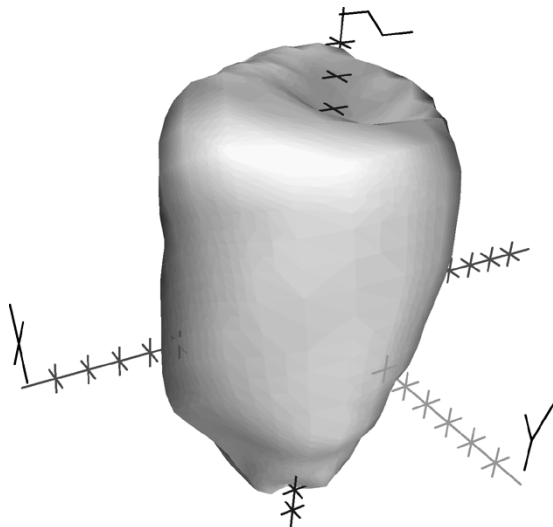


Fig. 5. Referential system for the left ventricle.  $Z$  is along the long axis, and  $XY$  planes are short axis.

### B. Data Processing

In those 2-D slices, the tagging grids and the resulting motion are extracted with a new fully automatic method [23]–[25]. For the 3-D motion, in the classical reference system defined by the “short axis” and “long axis” planes (see Fig. 5), our model can be decomposed in these two directions.

- 1) In the short-axis plane, we suppose a contraction/dilation and a rotation around the barycenter. Their amplitudes depend on  $z$ . We suppose a linear variation of the model parameters, between a reference basal slice, where no rotation is supposed,<sup>1</sup> and an apical slice.
- 2) In the long-axis plane, we suppose a homogeneous affine deformation, which lets the radiological apex still.

Then, the deformation is controlled by four temporal parameters: the apical contraction ( $C_A$ ), the basal contraction ( $C_B$ ), the longitudinal contraction ( $C_L$ ), and the apical rotation ( $\phi_A$ ). To eliminate the variation of the heartbeats between patients, some temporal resampling is done between end-diastole (ED,  $t = 0$ ) and end-systole (ES,  $t = 1$ , characterized by a minimal inner volume). Because of tag contrast dropout during the sequence in some cases, the curves are only computed for the first part of the diastolic relaxation. As the amplitude of the motion also varies between patients, each curve is normalized by its value at end-systole, and then the amplitudes and the normalized temporal curves are averaged separately. Figs. 6 and 7 show the four normalized motion curves of  $C_A$ ,  $C_B$ ,  $C_L$ , and  $\phi_A$ .

### C. Model Application

Let  $z_F$  be the  $z$ -coordinate of the radiological apex,  $z_A$  that of the apical slice, and  $z_B$  that of the basal slice. Then, the expression of the transformation of a vertex at cylindrical coordinates  $(r, \theta, z)$  in the LV referential is

$$\begin{cases} r \rightarrow \left( \frac{z-z_A}{z_B-z_A} C_B + \frac{z-z_B}{z_A-z_B} C_A \right) r \\ \theta \rightarrow \theta + \frac{z-z_B}{z_A-z_B} \phi_A \\ z \rightarrow C_L z + (1 - C_L) z_F. \end{cases} \quad (7)$$

<sup>1</sup>Studies show a maximal rotation angle of  $3^\circ$  [22], which is negligible for our application.

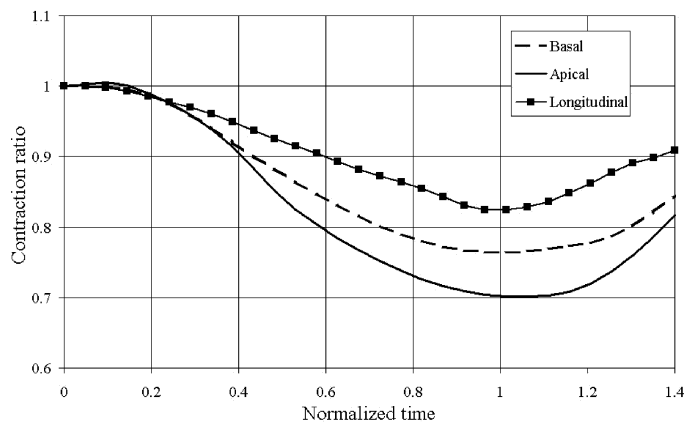


Fig. 6. Contraction curves for the mean model.

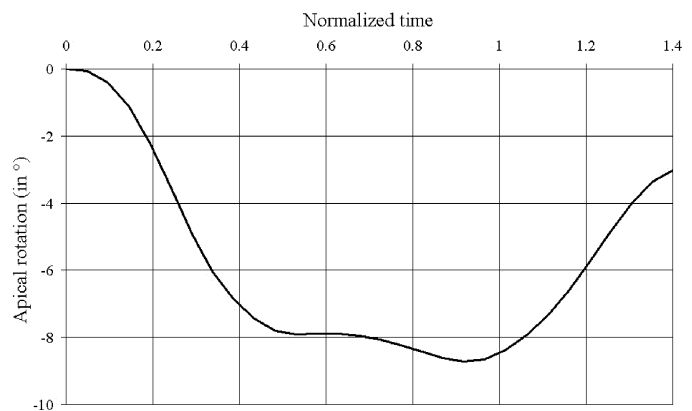


Fig. 7. Apical rotation (or twist) for the mean model.

This procedure is applied individually to all the mesh vertices, keeping its topology and the one-to-one correspondence over the cardiac cycle. Note also that this model can be applied between arbitrary phases of the cardiac cycle. In [26], we show that, although very compact, this model is quite realistic.

Fig. 8 shows the direct application of the motion model to the initial mesh, which is the end-diastolic one ( $t = 0$ ), already presented in Fig. 4. This figure clearly shows the usefulness of the proposed motion model, as the output meshes are close to the inner wall of the LV.

## IV. ANALYSIS TOOLS

As presented in the introduction (and on Fig. 1), the meshes derived from the motion model are further deformed using the 3DAO procedure of Section II in order to adapt to the image data.

Fig. 9 presents the final results, based on the meshes resulting from the motion model presented in Fig. 8. Since the “initial” meshes are close to the endocardium, the segmentation process is fast. Note that the 3DAO segmentation procedure is able to accurately capture the mitral valve plane, although the motion model overestimated its moving [compare views Fig. 9(a) and (b) with corresponding views Fig. 8(a) and (b)].

The resulting series of meshes is a discrete representation of a complex moving organ. One of the key advantages of this representation is the ease of computation of quantitative motion pa-

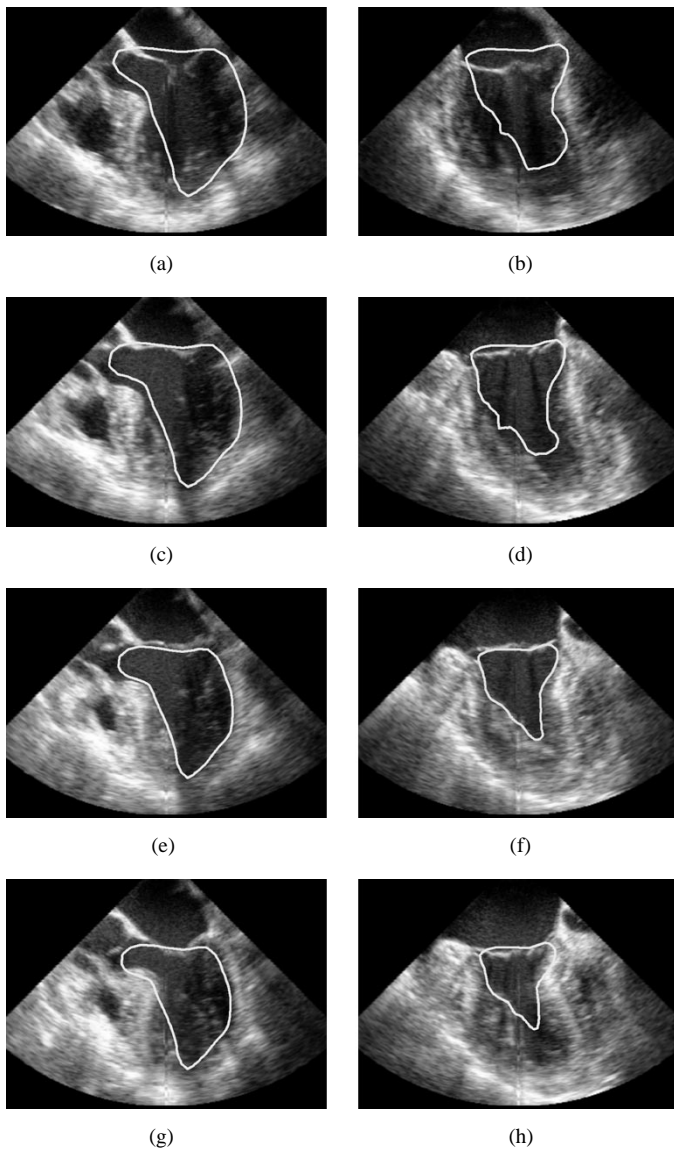


Fig. 8. Application of the motion model for successive times  $t = 0$  (ED), 4, 8, and 11 (ES). Two orthogonal views ( $v = 1$  and  $v = 2$ ) are displayed for each time frame, with the slice of the corresponding mesh surimposed. The reference frame is  $t = 8$ .

rameters. The usual global parameters are the global LV volume curve during the cardiac cycle, the ejection fraction, and the stroke. However, the analysis of the local wall motion is also of paramount importance in the diagnosis, in the followup of a pathology and of therapy efficiency. With the SM representation, both the local extent of the contraction (or relaxation) and its time of occurrence in the cardiac cycle can be accurately measured. Hence the contraction (or relaxation) abnormalities can be detected and quantified. This section describes the tools we have developed to analyze the result of the segmentation of the 3-D data sets.

The main idea is to quantify wall motion with the following measurements:

- 1) *deformation*: the signed distance  $\overline{BA}$  in millimeters, positive if contraction, negative if relaxation (see Fig. 10);
- 2) *strain*:  $|OB/OA| - 1$ , positive if contraction, negative if relaxation;

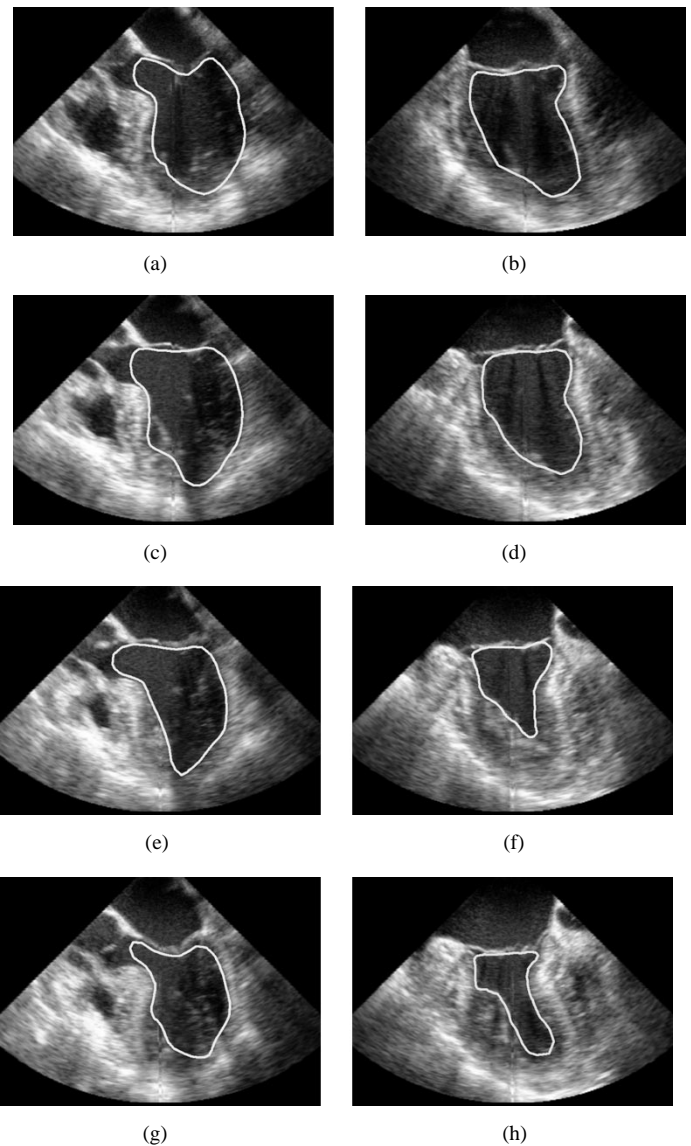


Fig. 9. Final result, after using the 3DAO procedure on the motion model result displayed in Fig. 8. Successive times  $t = 0$  (ED), 4, 8, and 11 (ES) are represented, each with two orthogonal views ( $v = 1$  and  $v = 2$ ) with the cross-section of the corresponding mesh superimposed.

- 3) *maximum motion time*: time corresponding to the largest motion (either in contraction or relaxation) with respect to a given reference time;

- 4) *local volume*: volume corresponding to the 3-D space between a bull's-eye region and the mesh center of gravity.

These computations are done for all the faces of the meshes. The 3-D distance computation can either be done "blindly," i.e., using each mesh as a separate discrete representation or using the vertices correspondence introduced by the motion model (see Section III).

The computations are done with respect to one "reference" time selected by the user, e.g., the end of diastole to study the systolic phase. The parameters correspond to the motion between a given mesh (i.e., the visible one) and the "reference" mesh. The global translation between the centers of gravity (CoGs) of both meshes can be compensated for. The deformation can be computed either radially from the CoGs

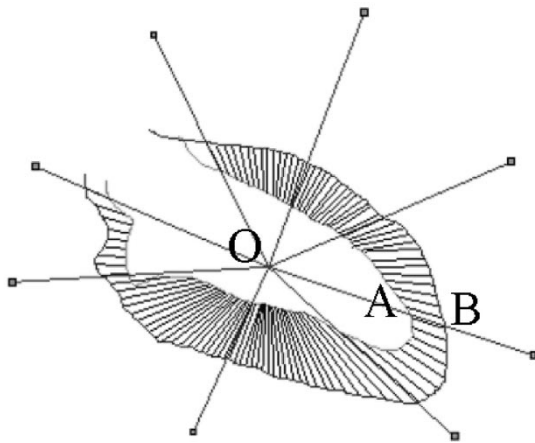


Fig. 10. 2-D view of the deformation computation (as in X-ray ventriculography). Point  $O$  is the center of gravity of the “reference” mesh (or of both meshes; see below).

or perpendicularly to the mesh surface (similar to Bolson and Sheehan “Centerline” and “CenterSurface” [27]). In practice, the combination of global translation compensation and CoG centered deformation leads to the most robust results.

The wall-motion measurements are averaged in each bull’s-eye region. In the average process, each face is weighted by its surface. Then these values are converted into colors, using a color map that can be adjusted by the user, and displayed simultaneously on the visible mesh and on the bull’s-eye representation [28], as shown in Fig. 15. The definition of the 16 polar regions of a bull’s-eye view is determined by the four key points already selected by the user to initialize the SM (see Section II), plus two points corresponding to the anterior and inferior part of the insertion of the right ventricle on the left ventricle. These last two points only define the septal regions of the bull’s eye and do not need to be accurately localized.

The deformation curves of a selected region over a cardiac cycle can also be displayed and compared. The contraction wave propagation can be assessed.

Fig. 15 shows a view of the wall-motion analysis tool.

## V. RESULTS

To validate the 3DAO segmentation procedure, *in vitro* volumetric experiments have been conducted using a beating balloon-in-balloon phantom [6]. This validation shows a volume measurement error of about 3%, always inferior to the protocol setup precision (5 ml), and a standard deviation inferior to 1.2 ml.

The results presented hereafter were obtained by using the following procedure (also depicted in Fig. 1).

- 1) For a given dataset, the segmentation process is initialized using one coarse LV mesh.
- 2) The 3DAO segmentation is applied (with the possibility for some user correction).
- 3) This segmentation is “propagated” to the rest of the sequence, using the motion model presented in Section III.
- 4) The 3DAO procedure is applied independently to each volume of the sequence under the user control.

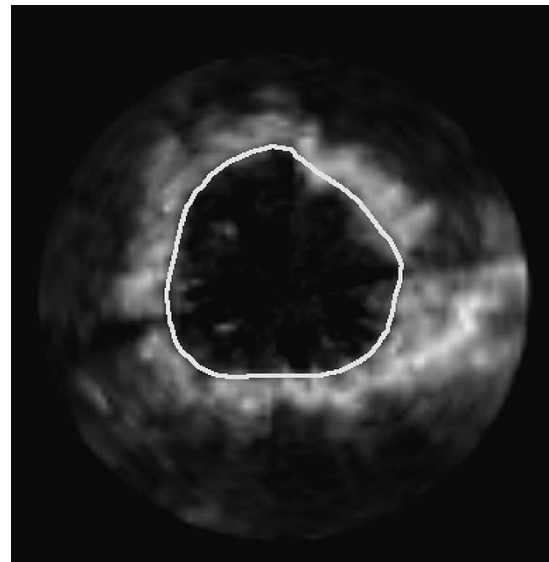


Fig. 11. Short-axis view of a 3-D gated-TEE dataset. The motion artifacts are clearly visible but are smoothed out by the 3DAO procedure.

To precisely capture the endocardium in one or several time frames, the user may find it necessary to modify the vertex density of the corresponding meshes. Then, the one-to-one correspondence introduced by the motion model is lost but our analysis tool (see Section IV) still works in this case.

All of Sections II and III are illustrated with one transesophageal echographic (TEE) datum, acquired using a ECG-gated mechanical scanhead, with an angular spacing of  $4^\circ$ . In the following, results obtained with two other TEE datasets are presented, followed by a recent result with the new Live 3-D system (Philips Medical System). The presented results are segmentation images with cross-sections of the mesh superimposed, because the segmentation is the critical part, whereas the subsequent quantitative analysis is rather straightforward.

### A. Results on ECG-Gated Data

First, two partial results are shown on another 3-D ECG-gated transesophageal echocardiography.

The first partial result, in Fig. 11, shows that the 3DAO procedure (Section II) is not disrupted by the clearly visible artifacts due to breathing and probe motion during the lengthy ECG-gated acquisition. These complex movements lead to artifacts in the 3-D reconstructed data that are very difficult to correct. Of course, these artifacts are best visible in reconstructed planes, i.e., the short-axis views in this example.

The second partial result, as shown in Fig. 12 on the same dataset, proves the usability of the motion model described in Section III, even in this very severe case of mitral regurgitation and LV remodeling.

Fig. 13 displays the segmentation results obtained with transthoracic data. Like TEE datasets, this dataset has been acquired using a motor-controlled scanhead, gated on the ECG. Note that the proposed approach is able to detect the endocardium on these low-quality data that exhibit severe echo dropout in the LV free wall part.

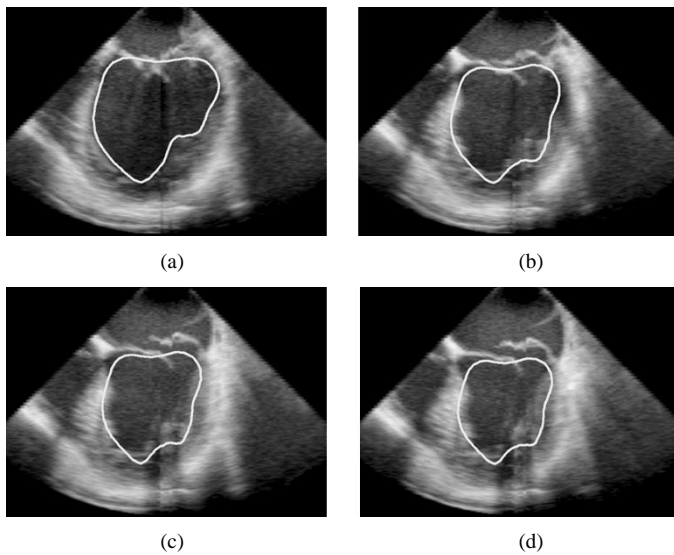


Fig. 12. Motion model applied to another TEE ECG-gated acquisition in a severe case of mitral valve regurgitation, between ED (reference) and ES, with the cross-section of the corresponding mesh superimposed.

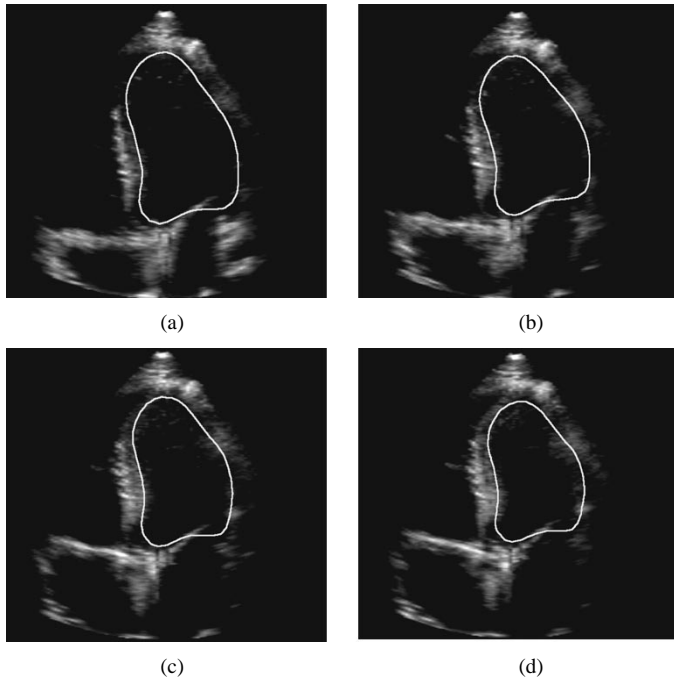


Fig. 13. Result on a very low-gain 3-D transthoracic acquisition, between ED and ES, with the cross-section of the corresponding mesh.

### B. Result on Live 3-D Data

Philips Medical System Andover has recently released the Live 3-D system,<sup>2</sup> based on a fully populated matrix array that is able to acquire 3-D volumes in real time without compromising the image quality. We present in Fig. 14 preliminary results obtained with this new image-acquisition protocol.<sup>3</sup>

Note that in the example, the papillary muscles are excluded from the inner volume of LV, whereas in the current practice, which relies on the adjustment of a crude model in one or two

<sup>2</sup>First presented during ASE'01 (Conference of the American Society of Echography), Seattle, WA, June 2001.

<sup>3</sup>Data reproduced with permission from Duke University by courtesy of Dr. J. Kisslo.

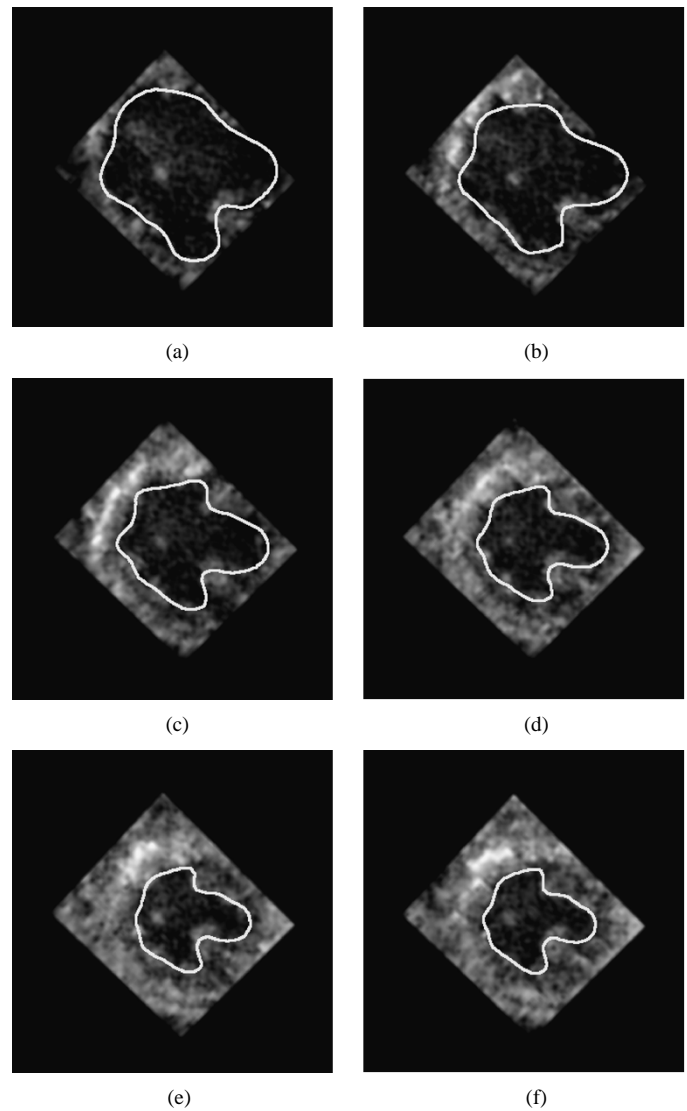


Fig. 14. Result on live 3-D dataset. Short-axis view at mid-LV level between ED and ES.

images, they are usually included in the LV. Although still debated, this choice seems to make more sense for the estimation of blood volumes. With our method, the papillary muscles could be included in the segmentation as well by increasing the global smoothness constraint (the internal forces of the 3 DAO procedure; see Section II). Fig. 12 shows a 3-D view of the segmentation result on this live 3-D data set.

## VI. CONCLUSION AND DISCUSSION

In this paper, we present a new and efficient method to quantify the LV function in 3-D echocardiography.

A method addressing the same problem has been recently proposed in [3], based on the tracking of the local echoes patterns in the myocardium. However, the results are obtained with open-chest dog heart data, which provide a level of image quality that is much better than that usually achieved in the transthoracic exams. Also the segmentation procedure is computationally intensive (3–4 h per dog).

Our method is fast: the whole procedure—including user interaction—takes less than 4 min on standard PC hardware. The

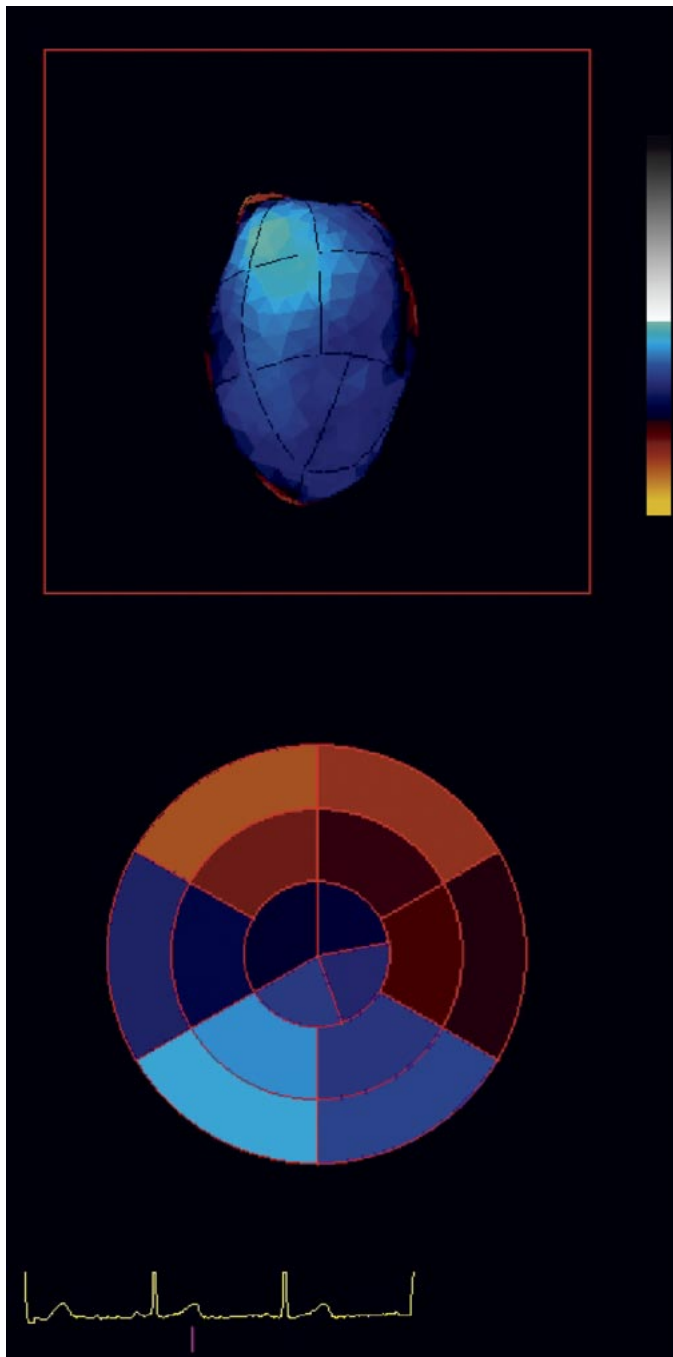


Fig. 15. Snapshot of 3-D analysis with the inferior part of colored mesh and the bull's-eye view.

segmentation step is model-driven in two ways. First (see Section II), the LV is represented by an active object whose deformations are mostly local. This kind of representation proves to be very flexible and able to depict a large variety of shapes. Secondly, we incorporate a global 4-D model (see Section III) that encompasses the normal motion of a beating LV. The combination of these local and global deformation approaches leads to a robust and efficient method that produces clinically pertinent LV function descriptors and that can cope with the limitations of ultrasound imaging.

Clinical validation of the volume measurement on ECG-gated acquisitions is currently under way at Freeman Hospital in New-



Fig. 16. 3-D view of the end-systolic live 3-D dataset with the corresponding segmentation result.

castle, U.K., using simultaneous Swan–Ganz catheter measurements on patients in an intensive care unit. This validation will also include comparisons with MRI studies on both the quantitative findings and the images themselves.

Clearly the emergence of real-time 3-D will speed up many of the clinical validations currently under way, as well as the deployment of 3-D echography in the clinical routine.

As a future improvement of this tool, we plan to add some capability of automatic comparison with a normal case, with reporting of contraction or relaxation problems, along with their position, extent, and timing.

As we have shown, a local deformation scheme is capable of capturing pathological cases. Moreover, we believe that adding a database of motion models may increase the method's robustness.

Another application we want to address is the 3-D assessment of the viability of the LV muscle in stress echo, which can be done automatically with much better reproducibility than in 2-D. Similar benefits can be expected in the study of the evolution of the LV function with time to assess its recovery. Wall-thickening measurements, which are more difficult because of the frequently poor definition of the epicardium, can also be addressed with the detection scheme proposed here, by incorporating the LV myocardium contraction into the cardiac deformation model. Also, taking benefit of other sources of information like tissue Doppler or contrast perfusion is certainly worth investigating.

#### ACKNOWLEDGMENT

The authors would like to acknowledge the participation of many people: F. Gerritsen and coworkers (Philips Medical System-Best); G. Schwartz, P. Detmer, and X. N. Li (PMS-Bothell); and K. Thiele and I. Salgo (PMS-Andover).

Data acquisition and clinical inputs were kindly provided by A. Kenny and coworkers (Freeman Hospital Newcastle, U.K.), Dr. J. Kisslo (Duke University), and Dr. B. Diebold (Hôpital Européen Georges Pompidou, Paris).

#### REFERENCES

- [1] O. Gérard, "Added value of real-time 3D imaging in cardiology," Laboratoires d'Electronique Philips (PRF), 2000-753, 2000.
- [2] A. S. Gopal *et al.*, "Assessment of cardiac function by three-dimensional echocardiography compared with conventional noninvasive methods," *Circulation*, vol. 92, pp. 842–853, 1995.
- [3] X. Papademetris, A. J. Sinusas, D. P. Dione, and J. S. Duncan, "Estimation of 3D left ventricular deformation from echocardiography," *Med. Image Anal.*, vol. 5, no. 1, pp. 17–28, 2001.
- [4] A. F. Frangi, W. J. Niessen, and M. A. Viergever, "Three-dimensional modeling for functional analysis of cardiac images: A review," *IEEE Trans. Med. Imag.*, vol. 20, no. 1, pp. 2–25, Jan. 2001.
- [5] A. F. Frangi, "Three-dimensional model-based analysis of vascular and cardiac images," Ph.D. dissertation, Utrecht Univ., the Netherlands, 2001.
- [6] O. Gérard, M. Fradkin, A. C. Billon, M. Jacob, J.-M. Rouet, J. M. Rouet, and S. Makram-Ebeid, "Automatic analysis of the left ventricle in the time sequence of 3D echo-cardiographic images," in *Medical Image Computing and Computer-Assisted Intervention (MICCAI'01)*, 2001, pp. 1224–1225.
- [7] J. Montagnat and H. Delingette, "Space and time shape constrained deformable surfaces for 4D medical image segmentation," in *Medical Image Computing and Computer-Assisted Intervention (MICCAI'00)*, 2000, pp. 196–205.
- [8] T. McInerney and D. Terzopoulou, "Deformable models in medical image analysis: A survey," *Med. Image Anal.*, vol. 1, no. 2, pp. 91–108, 1996.
- [9] J. Montagnat and H. Delingette, "A review of deformable surfaces: Topology, geometry and deformation," *Image Vision Comput.*, vol. 19, no. 14, pp. 1023–1040, Dec. 2001.
- [10] D. Terzopoulos and D. Metaxas, "Dynamic 3D models with local and global deformations: Deformable superquadrics," *IEEE Trans. Pattern Anal. Machine Intell.*, vol. 13, pp. 703–714, July 1991.
- [11] S. Menet, P. Sains-Marc, and G. Medioni, *B-Snakes: Implementation and Application to Stereo*. Amsterdam, the Netherlands: Elsevier Science, 1991, pp. 223–236.
- [12] A. Bulpitt and N. Eord, "An efficient 3D deformable model with a self optimizing topology," in *Br. Machine Vision Conf.*, 1995, pp. 37–46.
- [13] H. Delingette, "General object reconstruction based on simplex meshes," *Int. J. Comput. Vision*, vol. 32, no. 2, pp. 111–146, 1999.
- [14] C. Nastar and N. Ayache, "Frequency-based nonrigid motion analysis: Application to four dimensional medical images," *IEEE Trans. Pattern Anal. Machine Intell.*, vol. 18, pp. 1067–1079, 1996.
- [15] T. F. Cootes, C. J. Taylor, D. Cooper, and J. Graham, "Active shape models, their training and application," *Comput. Vision Image Understand.*, vol. 61, no. 1, pp. 38–59, Jan. 1995.
- [16] A. Neumann and C. Lorenz, "Statistical shape model based segmentation of medical images," *Comput. Med. Imag. Graph.*, vol. 22, pp. 133–143, 1998.
- [17] T. F. Cootes, G. J. Edwards, and C. J. Taylor, "Active appearance models," in *Proc. Eur. Conf. Computer Vision*, H. Burkhardt and B. Neumann, Eds., Springer 1998, pp. 484–498.
- [18] B. B. Kimia, A. Tannenbaum, and S. Zucker, "On the evolution of curves via a function of curvature, I: The classical case," *J. Math. Anal. Appl.*, vol. 163, pp. 438–458, 1992.
- [19] J. Montagnat, H. Delingette, and G. Malandain, "Cylindrical echocardiographic images segmentation based on 3D Deformable models," in *Medical Image Computing and Computer-Assisted Intervention (MICCAI'99)*, 1999, pp. 168–175.
- [20] S. E. Fischer, G. C. McKinnon, S. F. Msier, and P. Hoeiger, "Improved myocardial tagging contrast," *Magn. Reson. Med.*, vol. 30, pp. 191–200, 1993.
- [21] M. Stuber, M. A. Spiegel, and S. E. Fischer, "Single breath-hold slice-following CSPAMM myocardial tagging," *Magma*, vol. 9, pp. 85–91, 1999.
- [22] M. Stuber, E. Nagel, S. E. Fisher, M. A. Spiegel, M. B. Scheidegger, and P. Boesiger, "Quantification of the local heartwall motion by magnetic resonance myocardial tagging," *Camp. Med. Imag. Graph.*, vol. 22, pp. 217–228, 1998.
- [23] C. F. Allouche, "Automatic, real-time processing of SPAMM-tagged myocardium images," in *8th Annu. Conf. Time Int. Soc. Magnetic Resonance in Medicine*, Apr. 2001, p. 830.
- [24] C. F. Allouche, S. Makram-Ebeid, M. Stuber, N. Ayache, and H. Delingette, "New methods and algorithms for the accurate, real-time, motion analysis of the left ventricle with MRI tagging," in *Proc. Computer Assisted Radiology and Surgery (CARS)*, vol. 1231, Elsevier, June 2001, pp. 911–916.
- [25] C. F. Allouche, S. Makram-Ebeid, N. Ayache, and H. Delingette, "A new kinetic modeling scheme for the human left ventricle wall motion with MR-tagging imaging," presented at the 1st Int. Conf. Functional Imaging and Modeling of the Heart, Nov. 2001.
- [26] C. F. Allouche, "Reconstruction, recalage et modélisation 4D du mouvement de ventricule gauche du coeur humain pour le traitement d'images médicales," Ph.D. dissertation, Université Paris XI, 2002.
- [27] E. L. Bolson and F. H. Sheehan, "Centersurface model for 3D analysis of regional left ventricular functions," *Proc. IEEE Computers Cardiology*, pp. 735–738, 1993.
- [28] N. B. Schiller *et al.*, "Recommendations for quantitation of the left ventricle by two-dimensional echocardiography. American society of echocardiography committee on standards," *J. Amer. Soc. Echocardiogr.*, vol. 2, no. 5, pp. 358–367, 1989.